

基于可调光延迟线的微波光子零中频接收机研究

梅理^{1,2*}, 崇毓华^{1,2}, 朱宇鹏^{1,2}, 彭卫^{1,2}, 王冰^{1,2}

¹中国电子科技集团公司第三十八研究所, 安徽 合肥 230000;

²安徽省天线与微波工程实验室, 安徽 合肥 230000

摘要 提出了一种基于可调光延迟线的微波光子正交解调技术,并基于该技术设计了微波光子零中频接收机。通过调节光延迟线实现本振信号的 90°移相,并采用波分复用方法在共用的级联马赫-曾德尔调制器结构中实现两条正交链路的射频信号与本振信号的混频,从而提高了光正交解调的幅相一致性。所设计的微波光子零中频接收机可对光正交解调之后的中频处理器件如光电探测器、滤波器以及模数转换器等引起的链路幅相不平衡进行数字补偿。经数字幅相失衡补偿后,微波光子零中频接收机在中心频率为 12 GHz、瞬时带宽为 4 GHz 的工作频段内测得幅度不平衡小于 0.4 dB,相位不平衡小于 1.5°,镜频抑制度大于 45 dB,最高镜频抑制度可达 79 dB。

关键词 光通信;微波光子;宽带接收机;零中频;镜频抑制

中图分类号 TN29

文献标志码 A

doi: 10.3788/CJL202148.0906001

1 引言

数字接收机的工作带宽受限于模数转换器(ADC)的采样率,随着雷达、通信系统对工作带宽的要求不断提高,ADC的采样率逐渐成为数字接收机的性能瓶颈。超外差接收机受奈奎斯特采样定理限制,其工作带宽仅为 ADC 采样率的一半。零中频(zero-IF)接收机采用模拟正交解调技术,将射频(RF)信号转换为两路零中频 I/Q (in-phase/quadrature)信号进行数字采集,并可将接收机的工作带宽增大 1 倍^[1]。传统零中频接收机采用正交混频器实现零中频正交解调,正交混频器幅相失衡导致的镜频干扰严重减小了接收机的瞬时动态范围,限制了零中频接收机的应用^[2]。

近年来,应用微波光子技术解决宽带微波信号正交解调中幅相失衡的问题逐渐成为研究的热点^[3-6],在正交混频应用研究之外,还有大量的关于微波光子移相、变频以及微波光子链路基础性能提升的研究^[7-9]。目前主要的微波光子正交解调方法可分为三类:基于 90°光混频器的微波光子正交解调方法^[10-13],基于调制器偏置电压控制的正交解调

方法^[14-16],以及基于偏振控制器移相的正交解调方法^[17-18]。三种方法均通过电光调制器将射频与本振信号(LO)调制到光载波上进行光混频,区别在于 90°正交移相的实现方式不同。三种方法分别通过光混频器中的移相器、马赫-曾德尔调制器(MZM)以及偏振控制器实现对光场的相位调控,并通过光相干检测将光场相位调控转换为中频微波信号的相位调控。这些通过调节光场相位变化实现光载微波信号移相的方式,一般需要使用光滤波器或 I/Q 调制器来获得单边带光载微波信号,其中光滤波器的使用会限制微波光子正交解调的工作频率范围,I/Q 调制器在信号带宽较宽时的单边带调制效果会下降。在实际应用中,基于微波光子技术的零中频接收机还面临在光正交解调之后由对中频信号进行处理的元器件引入的额外幅相失衡的问题。

本文提出一种基于可调光延迟线移相的微波光子正交解调方法,该方法利用光延迟线实现光载本振信号的 90°移相,无需光滤波或复杂的单边带调制,通过光传输延迟实现微波信号的相位调控,受环境干扰影响更小。基于该方案设计了零中频接收机并对中频信号处理元件的幅相失衡进行数字补偿,

收稿日期: 2020-09-07; 修回日期: 2020-10-21; 录用日期: 2020-11-18

基金项目: 国家重点研发计划(2019YFB2203201)

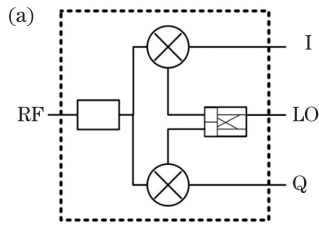
*E-mail: meili@mail.ustc.edu.cn

实现了瞬时处理带宽为 4 GHz、镜频抑制优于 45 dB、工作频段覆盖 10~14 GHz 的微波光子零中频接收机。

2 基本原理

2.1 正交混频原理

传统零中频接收机中使用的正交混频器的原理如图 1(a)所示,射频信号功分两路后分别与两路相位相差 90°的本振信号进行混频,得到两路正交的中频 I/Q 信号,本振信号频率与射频信号中



心频率相同时即可实现零中频正交解调。图 1(b)为零中频正交解调原理示意图,宽带射频信号中心频率与本振信号频率相同时,两信号混频后形成的中频信号与镜频信号频谱相重叠。在正交解调中,通过将 I/Q 两路正交的中频信号合并为复信号,可消除镜频信号的干扰。由于电子器件在宽带范围内的幅相一致性难以保证,射频信号功分器、本振信号的功分和移相以及两路混频器的一致性差异,均会引起中频 I/Q 信号的幅相不平衡。

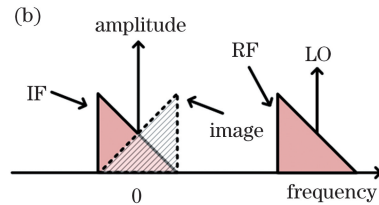


图 1 正交混频器原理图和零中频混频示意图。(a)正交混频器原理示意图;(b)零中频混频示意图

Fig. 1 Schematic diagram of I/Q mixer and diagram of zero-IF mixing. (a) Schematic diagram of I/Q mixer; (b) diagram of zero-IF mixing

考虑混频器宽带幅相误差后的 I/Q 输出信号可表示为

$$\begin{cases} I_{FI} = \sin(\omega_{IF}t + \varphi_{RF}) \\ I_{FQ} = k_s \cdot k_h \cdot \cos(\omega_{IF}t + \varphi_{RF} + \varphi_s + \varphi_h) \end{cases}, (1)$$

式中: I_{FI} 与 I_{FQ} 表示正交混频器解调出的两路中频信号; ω_{IF} 为中频信号频率,等于射频信号中心频率与本振信号频率之差,零中频接收时 $\omega_{IF}=0$; φ_{RF} 为射频信号的相位调制项; k_s 与 φ_s 表示由射频功分器引入的两路射频信号幅度相位差,两参数均与射频信号的频率相关; k_h 与 φ_h 表示由 90°电桥引入的两路本振信号间的幅度差和相对于 90°移相的相位差。I/Q 链路存在幅相不平衡时,零中频接收的镜频抑制仿真结果如图 2 所示。图 2(a)为 I/Q 幅相不平衡参数设置,图中 f_{IF}/f_{BW} 表示中频信号频率

与工作带宽的比值。可以看出,幅度不平衡值为-0.3 dB~0.7 dB 并在工作带宽内随频率呈线性变化,相位不平衡值为-5°~15°并在工作带宽内呈线性变化。零中频接收后的 I/Q 信号频谱如图 2(b)所示,选取工作带宽内 20 个频点对解调后的 I/Q 信号进行频谱分析,图中星号标记为正交解调后的 20 个中频信号峰值,圆形标记为相应的镜频信号峰值。幅相误差最大时,镜频干扰导致接收机的动态范围小于 20 dB,这严重影响了宽带零中频接收机的工程应用。在微波光子处理中,由于微波信号带宽远小于光载频,信号相对带宽极小,因此在光载波上对微波信号进行处理时几乎不存在与微波频率相关的幅相一致性差异,可实现高镜频抑制的宽带微波信号正交解调。

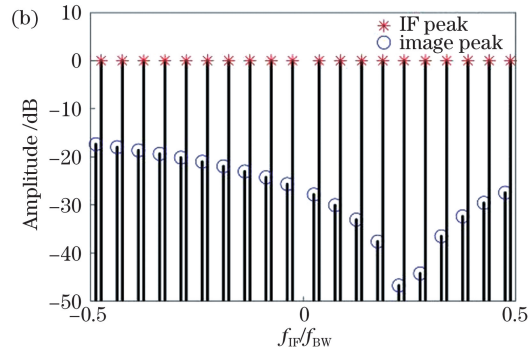
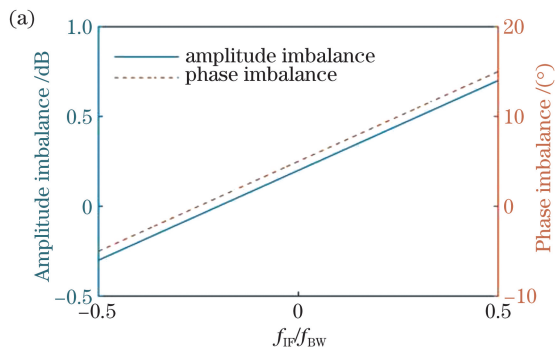


图 2 零中频正交解调仿真。(a) I/Q 信号的幅相不平衡;(b) 20 个不同频率射频信号经正交解调后的频谱分析结果

Fig. 2 Simulation results of zero-IF quadrature modulation. (a) Amplitude and phase imbalances of I/Q signal; (b) frequency spectra of 20 RF signals after orthogonal demodulation

2.2 基于可调光延迟线的微波光子正交解调原理

微波光子正交解调原理框图如图 3 所示,通过级联两个 MZM 的方式实现本振信号与射频信号的混频。将本振信号通过第一级 MZM 加载到由波分复用器(WDM)合束的两路波长不同的光载波上。解波分复用后通过可调光延迟线(TODL)调节两路光载波本振信号的相对传输延迟,使得 Q 路本振光信号相比 I 路的传输延迟为本振信号周期的 1/4,再次经波分复用合路后 Q 路光载波上的微波本振信号相比 I 路本振信号存在 90°相位延迟。射频信号通过第二级 MZM 与正交本振信号混频,混频后的光信号经掺铒光纤放大器(EDFA)的放大后被解复用为光 I/Q 信号,通过可调衰减器(TA)和光延迟线

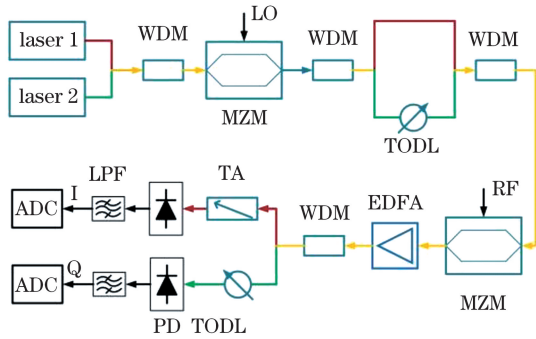


图 3 基于 TODL 的微波光子正交解调原理图
Fig. 3 Schematic diagram of microwave photonic orthogonal demodulation based on TODL

调整两路信号的幅度和传输延迟。两路光 I/Q 信号经光电转换、低通滤波器(LPF)后,高频信号被滤除。通过两路 ADC 进行数字采集,并完成后续的数字幅相补偿。

在本方案中,两路不同波长的信号所经过的链路基本一致,这里以 Q 路信号为例分析光 I/Q 解调过程。输入的射频信号与本振信号分别可表示为: $v_{RF} = V_{RF} \sin[\omega_{RF}t + \varphi_{RF}(t)]$, $v_{LO} = V_{LO} \sin(\omega_{LO}t)$, 其中 V_{RF} 与 V_{LO} 分别为射频与本振信号的幅度, ω_{RF} 与 ω_{LO} 分别为射频与本振信号的角频率, $\varphi_{RF}(t)$ 表示射频信号的相位调制项。Q 路激光器的输出光功率为 P_0 , 忽略波分复用器与调制器的插损,对第一级 MZM 加载本振信号后,调制器工作于正交偏置点时输出的 Q 路光信号为

$$P_{MZM1} = \frac{1}{2} P_0 \left[1 + \sin\left(\frac{\pi}{V_{\pi}} v_{LO}\right) \right], \quad (2)$$

式中: V_{π} 为调制器的半波电压。小信号近似下,对(2)式进行贝塞尔展开并忽略高阶项:

$$P_{MZM1} = \frac{1}{2} P_0 \left[1 + \frac{\pi}{V_{\pi}} V_{LO} \sin(\omega_{LO}t) \right]. \quad (3)$$

Q 路光信号经可调光延迟线的 1/4 周期相对延迟后的表达式为

$$P_{ODL} = \frac{1}{2} P_0 \left[1 + \frac{\pi}{V_{\pi}} V_{LO} \sin\left(\omega_{LO}t - \frac{\pi}{2}\right) \right]. \quad (4)$$

假设两个调制器的半波电压相同,当对第二级调制器加载射频信号后,Q 路光信号可近似为

$$P_{MZM2} = \frac{1}{4} P_0 \left[1 + \frac{\pi}{V_{\pi}} V_{LO} \sin\left(\omega_{LO}t - \frac{\pi}{2}\right) \right] \left\{ 1 + \frac{\pi}{V_{\pi}} V_{RF} \sin[\omega_{RF}t + \varphi_{RF}(t)] \right\}. \quad (5)$$

经过光放大、光电转换并滤除高频信号后,零中频解调得到的 Q 路中频信号可表示为

$$v_Q = \frac{1}{8} G \cdot \eta \cdot R_L \cdot P_0 \cdot \frac{\pi}{V_{\pi}} V_{LO} \cdot \frac{\pi}{V_{\pi}} V_{RF} \cdot \cos\left[\varphi_{RF}(t) + \frac{\pi}{2}\right], \quad (6)$$

式中: G 表示 EDFA 引入的光增益; η 为光电探测器的转换效率; R_L 为探测器的输出负载阻抗。

I 路信号传输过程与 Q 路相似,不同点在于:两级 MZM 之间, I 路信号不存在光延迟线引入的相对延迟。假设 I 路激光器的输出功率也为 P_0 , 则 I 路输出的中频信号可表示为

$$v_I = \frac{1}{8} G \cdot \eta \cdot R_L \cdot P_0 \cdot \frac{\pi}{V_{\pi}} V_{LO} \cdot \frac{\pi}{V_{\pi}} V_{RF} \cdot \cos[\varphi_{RF}(t)]. \quad (7)$$

对比(6)式与(7)式可发现, I 路与 Q 路中频信号的幅度、相位调制一致且相位相差 90°。光正交解调研究中通常采用控制光信号相位的方法调控混频后的中频信号相位,这种方式需要对光信号进行精准移相,难度较大且易受环境干扰。本文通过光传输延迟的方式实现本振信号的 90°移相,相位调控在微波频段完成,受环境影响较小。使用光延迟线进行本振移相时,对不同频率的本振信号进行 90°移相所需的延迟量也不同。因此,光延迟线需具有一定的延迟范围以匹配所设计的工作频段,同时移相的精度也由延时的精度决定。此外,结合波分复用方法, I/Q 两路信号混频过程中,微波射频信号与本振信号通过共用的级联 MZM 结构实现光混频,正交解调过程中的 I/Q 幅相一致性得到了保障。

3 实验结果与分析

根据图 3 的方案进行实验,半导体激光器(大族锐波 RP-FM-33/34-0080)的中心波长分别选取 1550.12 nm 和 1550.92 nm,输出功率为 80 mW;波分复用器选择通带中心波长为 1550.12 nm 的保偏波分复用器,通过波分复用器反射端对 1550.92 nm 的光信号进行合路与分路;调制器(EOSPACE AX-0MKS-20-PFA-PFA-LV) 3 dB 射频带宽大于 18 GHz。调制器具有一定的波长相关性,对于不同波长的光源,调制器的正交工作点偏置电压会有差异。选用频率间隔为 100 GHz 的光源进行波分复用,避免了 MZM 波长相关性的影响,同时也保证了较高的通道隔离度。由于链路光插损较大,因此在第二级 MZM 调制器后使用掺铒光纤放大器(脉锐

光电 EDFA-BA-20-M)进行增益补偿。电控光延迟线(欧爱西 MODL-300)的最大延迟量为 330 ps,延迟步进为 0.067 ps。

由于链路设计及链路中各器件波长相关性的影响,两条链路对射频信号的变频损耗并不完全相同。从两个 PD 输出端口分别测试中频信号强度,通过调节可调光衰减器即可将 I/Q 链路的变频损耗调节为一致。图 4 为调节后的链路变频损耗测试结果。图 4(a)为射频信号强度($I_{RF,in}$)为 5.5 dBm 时,通过改变本振信号强度($I_{LO,in}$)得到的变频损耗曲线,本振信号在 1 dB 压缩点处的强度约为 8.8 dBm。取本振信号强度为 8.8 dBm 时,通过改变射频信号强度得到如图 4(b)所示的变频损耗曲线,射频信号的 1 dB 压缩点为 10.8 dBm,此时对应的链路变频损耗约为 31 dB。

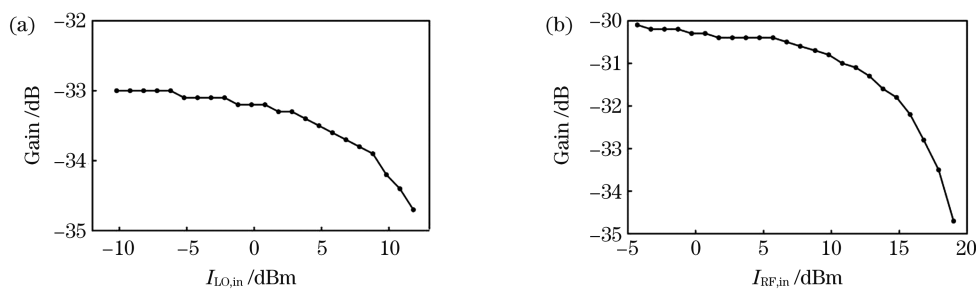


图 4 微波光子链路变频损耗测试。(a)射频信号强度为 5.5 dBm 时,变频损耗随本振信号强度的变化;(b)本振信号强度为 8.8 dBm 时,变频损耗随射频信号强度的变化

Fig. 4 Conversion loss of microwave photonic link. (a) Conversion loss versus amplitude of LO signal when intensity of RF signal is 5.5 dBm; (b) conversion loss versus amplitude of RF signal when intensity of LO signal is 8.8 dBm

在光正交解调之后,零中频接收机中的中频光信号需经光电转换、低通滤波以及 ADC 采集才能被转换为数字 I/Q 信号。由于各光电器件的一致性差异,两路 I/Q 信号间会引入额外的幅相不平衡,因此需要通过数字后处理技术进行补偿。实验中所用的光电探测器、低通滤波器以及 ADC 的幅相一致性测试结果如图 5 所示。所使用的滤波器为截止频率为 2 GHz 的低通滤波器(泰格 TGF-D1120-007),在通带内的幅度一致性差异 < 0.3 dB,相位一致性差异 $< 2.5^\circ$ 。光电探测器(中国电子科技集团公司第四十四研究所研制的 GD45220R)在直流到 2 GHz 工作频段内的幅度一致性差异 < 1.2 dB,相位一致性差异 $< 3.5^\circ$ 。数字采集芯片(德州仪器 ADC12DL3200)的采样率设置为 4 GSa/s,量化位数为 12 bit。向两个 ADC 同时注入两路同频率的信号,改变信号频率并采集数据,通过计算得到两片 ADC 的幅相一致性,如图 5(e)、(f)所示。两条数字采集链路的幅度一致性

差异 < 3.8 dB,相位一致性差异 $< 20^\circ$ 。数字采集电路在 250 MHz 左右存在响应奇点,使得 250 MHz 附近的 ADC 幅相一致性严重恶化。

使用上述光电器件及数字采集链路搭建了基于可调光延迟线的微波光子零中频接收机,本振信号频率设为 12 GHz,所使用的可调光延迟线的步进为 67 fs,理论上在 12 GHz 频点的移相精度可达 0.29° 。射频信号以 4 MHz 为步进,在 10~14 GHz 间的一系列频点处采集数据。通过分析各频点解调后的 I/Q 信号幅度、相位差,可得到本振信号的移相误差、链路长度不同引起的传输延迟误差以及由器件一致性差异引起的幅相不平衡。通过调节第一级光延迟线使 12 GHz 本振信号移相接近 90° ,并调节第二级光延迟线以使 I/Q 链路长度相同,重复采集两组 10~14 GHz 间射频信号的正交解调数据,以一组为校正信号生成幅相校正参数,用于修正第二组正交解调数据。

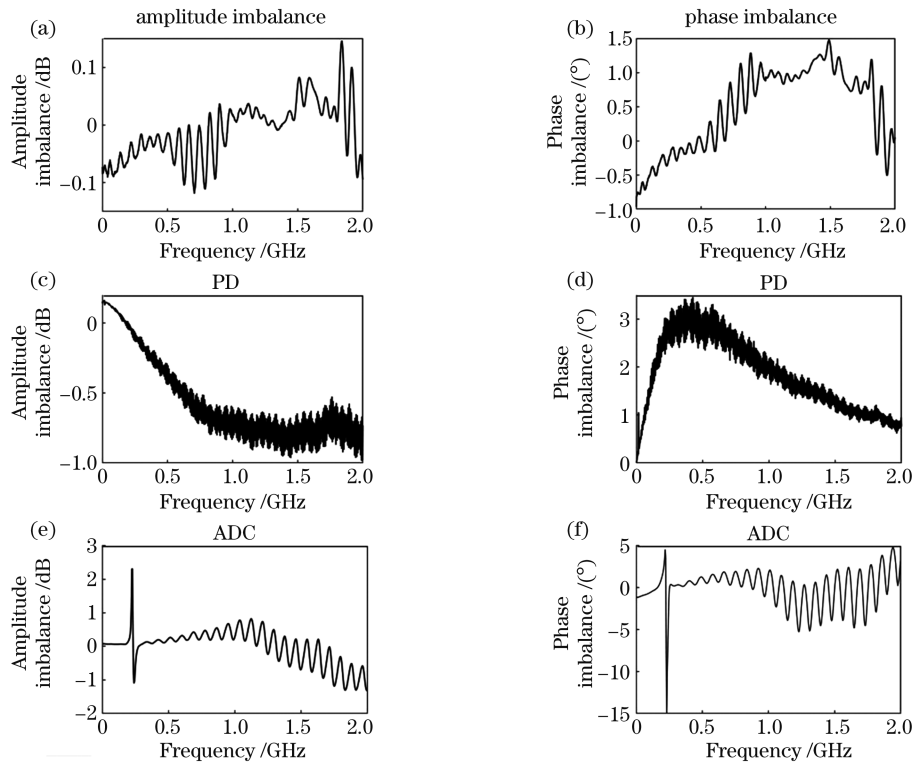


图 5 I/Q 链路各器件的幅相一致性测试结果。(a)(b)低通滤波器;(c)(d) PD;(e)(f) ADC

Fig. 5 Test results of amplitude and phase consistency of devices in I/Q links. (a) (b) Low-pass filter; (c) (d) PD; (e) (f) ADC

如图 6(a)、(b)所示,未对 PD 等光电器件引入的中频幅相失衡进行校正时,链路的幅度不平衡约为 4 dB,相位不平衡约为 40°。图 6(c)为对 10~14 GHz 工作频段内均匀分布的 20 个频点的正交解调信号进行频谱分析的结果,以 I 路信号为实部、Q 路信号为虚部构建复中频信号并进行傅里叶变

换,得到其频谱。频谱中,中频信号用星号标记,镜频干扰信号用圆圈标记,镜频信号的强度远高于底噪,使得接收机的瞬时动态信号大幅降低。图 6(d)为选取工作带宽内 200 个频点进行零中频接收后计算的镜频抑制度分布,受各器件幅相一致性的影响,接收机的镜频抑制度最小值仅为 18 dB。

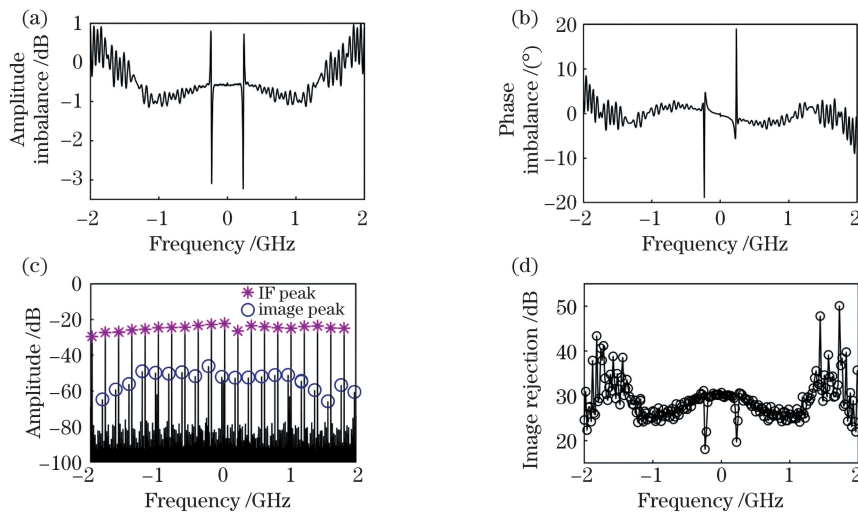


图 6 无中频幅相校正时,微波光子零中频接收机测试结果。无校正时, I/Q 链路的(a)幅度不平衡和(b)幅相不平衡;(c)20 个不同频点射频信号的零中频采集结果;(d)无中频幅相校正时接收机镜频抑制度

Fig. 6 Experimental results of microwave photonic zero-IF receiver without IF amplitude/phase calibration. (a) Amplitude imbalance and (b) phase imbalance of I/Q link without calibration; (c) results of 20 different RF signals acquired by zero-IF acquisition; (d) image rejection of zero-IF receiver without IF amplitude and phase calibration

基于图 6(a)、(b)所示的幅相不平衡数据,可拟合得到中频幅相校正参数。进行中频幅相校正后的 I/Q 幅相不平衡如图 7(a)、(b)所示,在 4 GHz 工作带宽内,I/Q 链路校正后的幅度不平衡 <0.4 dB,相位不平衡 $<1.5^\circ$,远小于校正前的链路幅相不平衡。经中频幅相校正后可进一步通过构建 I/Q 失衡补偿滤波器进行幅相补偿^[19],修正后的零中频接收结果如图 7(c)、(d)所示。图 7(c)为在 10~14 GHz 工作频段内的 20 个频点进行零中频接收后的频谱分析结果。频谱中,中频信号用星号标记,镜频干扰用

圆圈标记,可以看出经中频幅相校正后的镜频干扰信号与接收机的谐波杂散噪声处于同一水平。图 7(d)为选取工作带宽内 200 个频点进行零中频接收后计算得到的镜频抑制度。在全工作带宽内,接收机的镜频抑制度均 >45 dB,最高镜频抑制度接近 80 dB。根据图 7(a)、(b)所示的 I/Q 幅相不平衡,经数字 I/Q 失衡补偿后接收机的镜频抑制度应在 50 dB 以上,但光传输链路的幅相稳定性造成接收机幅相不平衡特性随时间的推移而变化,这影响了数字幅相修正效果。

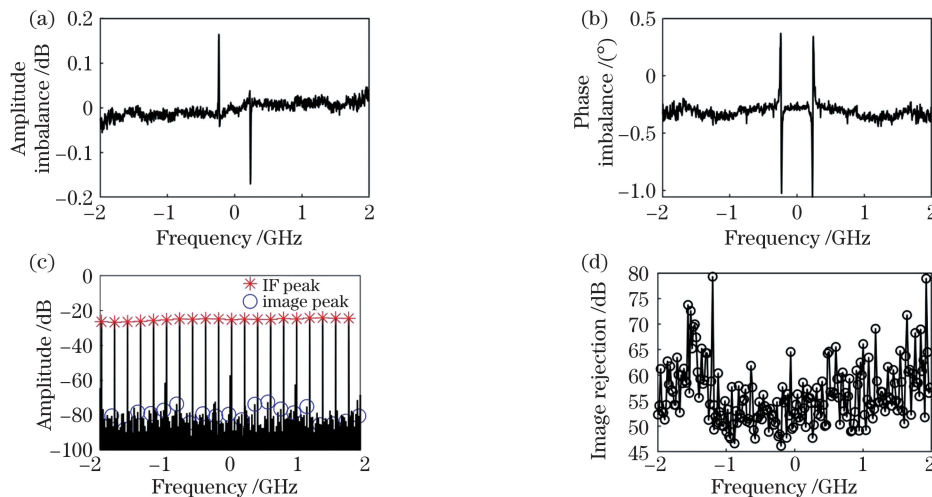


图 7 中频幅相校正后,微波光子零中频接收机的测试结果。校正后 I/Q 链路的(a)幅度不平衡和(b)相位不平衡;(c) 20 个不同频点射频信号的零中频采集结果;(d)接收机镜频抑制度

Fig. 7 Experimental results of microwave photonic zero-IF receiver after IF amplitude and phase calibration. (a) Amplitude imbalance and (b) phase imbalance of I/Q link after calibration; (c) results of 20 different RF signals acquired by zero-IF acquisition; (d) image rejection of zero-IF receiver

4 结 论

提出了一种基于可调光延迟线的微波光子正交解调方法,与已有的光正交解调方法相比,该方法通过光传输延迟的方式在微波频段实现本振信号的 90° 移相,受环境干扰影响较小。通过波分复用的微波光子链路设计,在共用的级联 MZM 结构中实现 I/Q 链路的射频、本振信号光混频,从而提高了光正交解调的宽带幅相一致性。已有的微波光子正交混频研究对光正交解调后的光电转换、低通滤波以及数字采集器件引入的 I/Q 幅相不平衡关注较少。设计了基于可调光延迟线的微波光子零中频接收机,对中频信号处理引入的 IQ 幅相不平衡进行校正后,测得链路的幅度不平衡 <0.4 dB,相位不平衡 $<1.5^\circ$,这验证了宽带光 IQ 解调高幅相一致性的特点。零中频接收机在 10~14 GHz 工作频段内的镜频抑制度 >45 dB,最高镜频抑制度可达 79 dB,通

过提高光链路的幅相稳定性可进一步提升接收机的带内镜频抑制度。

参 考 文 献

- [1] Skolnik M I. Introduction to radar systems[M]. Zuo Q S, Xu G L, M L, et al., Transl. 3rd ed. Beijing: Electronic Industry Press, 2006: 552-562.
美林·斯科尼克. 雷达系统导论[M]. 左群声, 徐国良, 马林, 等, 译. 3 版. 北京: 电子工业出版社, 2006: 552-562.
- [2] Fan H H, Wu X B, Sun W J. Design of a broadband T/R module integrating RF and digital circuits[J]. Radar Science and Technology, 2020, 18(3): 340-344, 350.
范欢欢, 伍小保, 孙维佳. 一种射频数字一体化宽带收发模块设计[J]. 雷达科学与技术, 2020, 18(3): 340-344, 350.
- [3] Lu B, Pan W, Zou X H, et al. Wideband microwave Doppler frequency shift measurement and direction

- discrimination using photonic I/Q detection [J]. *Journal of Lightwave Technology*, 2016, 34(20): 4639-4645.
- [4] Zhang J, Chan E H W, Wang X, et al. High conversion efficiency photonic microwave mixer with image rejection capability [J]. *IEEE Photonics Journal*, 2016, 8(4): 1-11.
- [5] Ridgway R W, Dohrman C L, Conway J A. Microwave photonics programs at DARPA [J]. *Journal of Lightwave Technology*, 2014, 32(20): 3428-3439.
- [6] Gao Y S, Wen A J, Zhang W, et al. Ultra-wideband photonic microwave I/Q mixer for zero-IF receiver [J]. *IEEE Transactions on Microwave Theory and Techniques*, 2017, 65(11): 4513-4525.
- [7] Li C X, Zhang B F, Lu L, et al. Microwave photonic frequency conversion and phase-shifting technology of photoelectronic oscillator loop[J]. *Chinese Journal of Lasers*, 2019, 46(1): 0101001.
李诚鑫, 张宝富, 卢麟, 等. 光电振荡环路的微波光子变频与移相技术研究[J]. *中国激光*, 2019, 46(1): 0101001.
- [8] Li Q, Du C, Li X, et al. Microwave photonic down-conversion system based on stimulated Brillouin scattering effect [J]. *Chinese Journal of Lasers*, 2019, 46(7): 0701006.
李强, 都聪, 李想, 等. 基于受激布里渊散射效应的微波光子下变频系统[J]. *中国激光*, 2019, 46(7): 0701006.
- [9] Zhao F, Cai W T, Zhang L L, et al. Linearization analysis of microwave photonic link based on balanced detection[J]. *Acta Optica Sinica*, 2019, 39(11): 1104001.
赵峰, 蔡卫童, 张龙龙, 等. 基于平衡探测的微波光子链路线性化分析[J]. *光学学报*, 2019, 39(11): 1104001.
- [10] Tang Z Z, Pan S L. A reconfigurable photonic microwave mixer using a 90° optical hybrid[J]. *IEEE Transactions on Microwave Theory and Techniques*, 2016, 64(9): 3017-3025.
- [11] Tang Z, Pan S. Reconfigurable microwave photonic mixer with minimized path separation and large suppression of mixing spurs [J]. *Optics Letters*, 2017, 42(1): 33-36.
- [12] Li J Q, Xiao J, Song X X, et al. Full-band direct-conversion receiver with enhanced port isolation and I/Q phase balance using microwave photonic I/Q mixer[J]. *Chinese Optics Letters*, 2017, 15(1): 010014.
- [13] Meng Z Y, Li J Q, Yin C J, et al. Dual-band dechirping LFM CW radar receiver with high image rejection using microwave photonic I/Q mixer [J]. *Optics Express*, 2017, 25(18): 22055-22065.
- [14] Tang Z Z, Pan S L. Photonic microwave image-reject mixer with large suppression of mixing spurs [C]//2016 IEEE MTT-S International Microwave Symposium (IMS), May 22-27, 2016, San Francisco, CA, USA. New York: IEEE Press, 2016: 1-4.
- [15] Shi J Z, Zhang F Z, Ben D, et al. Wideband microwave photonic I/Q mixer based on parallel installed phase modulator and Mach-Zehnder modulator [C]//2018 IEEE MTT-S International Wireless Symposium (IWS), May 6-10, 2018, Chengdu, China. New York: IEEE Press, 2018: 1-4.
- [16] Gao Y S, Wen A J, Jiang W, et al. Wideband photonic microwave SSB up-converter and I/Q modulator [J]. *Journal of Lightwave Technology*, 2017, 35(18): 4023-4032.
- [17] Gao Y, Wen A, Tu Z, et al. Simultaneously photonic frequency down conversion, multichannel phase shifting, and IQ demodulation for wideband microwave signals [J]. *Optics Letters*, 2016, 41(19): 4484-4487.
- [18] Gao Y S, Wen A J, Jiang W, et al. All-optical and broadband microwave fundamental/sub-harmonic I/Q down-converters[J]. *Optics Express*, 2018, 26(6): 7336-7350.
- [19] Cheng C H, Liou L L, Lin D M, et al. Wideband in-phase/quadrature imbalance compensation using finite impulse response filter [J]. *IET Radar, Sonar & Navigation*, 2014, 8(7): 797-804.

Optical Delay Line-Based Microwave Photonic Zero-Intermediate-Frequency Receiver

Mei Li^{1,2,*}, Chong Yuhua^{1,2}, Zhu Yupeng^{1,2}, Peng Wei^{1,2}, Wang Bing^{1,2}

¹The 38th Research Institute of China Electronics Technology Group Corporation, Hefei, Anhui 230000, China;

²Anhui Province Engineering Laboratory for Antennas and Microwave, Hefei, Anhui 230000, China

Abstract

Objective The next-generation radar systems make increasing demands on receivers, such as large instantaneous bandwidth for increased resolution, wide operating frequency for multi-function, and high radio frequency (RF) isolation for large-scale phased array antenna systems. These demands are enormous for electronic receiver technologies. Owing to the advantages of large bandwidth, high isolation, and immunity to electromagnetic interference, photonic-assisted microwave processing techniques provide new solutions for radar receivers. A zero-intermediate-frequency (IF) in-phase and quadrature (I/Q) receiver using microwave photonic technology, exploiting the advantages of the ultrawideband photonic processing technology and agile electronic digital processing technology, has become a competitive solution for wideband radar systems. Recent studies on microwave photonic I/Q receivers obtain the 90° phase shift between I/Q signals by adjusting the phase of signals in optical frequency. Commonly employed optical phase shift methods, such as using an optical 90° hybrid or adjusting a polarization controller, experience disturbance of temperature and stress. In these methods, a narrow bandpass optical filter or complicate electronic-optical modulation is needed for carrier-suppressed single-sideband modulation, which restricts the operation frequency of photonic I/Q receivers. Besides, the amplitude and phase imbalances of the I/Q channels induced by the IF processing devices, such as photodiodes (PDs), low-pass filters, and analog-to-digital converters (ADCs) are rarely considered recently. Our research on a simple and stable microwave photonic I/Q receiver has potential in radar detection applications.

Methods By converting input RF signal into zero IF signals with an I/Q mixer, the I/Q receiver can realize cancellation of image interference, thus doubling receiver's working bandwidth (Fig. 1). However, as it is hard for electronic devices to keep high amplitude and phase consistency in wide bandwidth, the image cancellation decreases in ultrawideband receiver. The image rejection ratio will fall to less than 20 dB with -0.3–0.7 dB amplitude imbalance and -5°–15° phase imbalance (Fig. 2). In our research, the I/Q mixer is realized with optical devices and the imbalance of devices following the optical mixer in I/Q channels is compensated with digital processing, thus realizing high image rejection in 4 GHz operation bandwidth. An optical delay line (ODL) is used for phase tuning of microwave signals carried by optical field (Fig. 3). Two continuous-wave lasers working at 1550.9 and 1550.1 nm separately are combined through a wavelength division multiplexer (WDM) and sent to a Mach-Zehnder modulator (MZM). A local oscillator (LO) signal is used as the optical carrier through the MZM. The output signal is then wavelength-demuxed and multiplexed by two WDMs. An equivalent 90° phase shift between the LO signals carried on the two optical wavelengths can be introduced by tuning the ODL on one of the wavelength channels between the two WDMs. An RF signal is applied to the combined optical signals through a second MZM. An erbium-doped fiber amplifier is used to compensate for the link loss, and then the two optical signals are separated through a WDM to obtain I/Q signals. The relative amplitude difference and transmission delay between the I/Q channels are adjusted through a tunable attenuator and another optical delay line on the two optical paths separately. After being detected by two PDs, the I/Q signals are filtered by 2 GHz low-pass microwave filters and then sampled by two ADCs working at 4-GSa/s sampling rate. We generate a series of RF signals with different frequencies from 10 to 14 GHz and set the LO signal frequency at 12 GHz. The I/Q signals are acquired twice to form the calibration and signal data groups. The amplitude and phase imbalances of the I/Q channels induced by the IF processing devices can be obtained by analyzing the calibration data group.

Results and Discussions The input 1-dB compression powers of LO and RF signals are 8.8 and 10.8 dBm, respectively, and the conversion loss of the microwave photonic link is 31 dB (Fig. 4). In our receiver, the filters, PDs, and ADCs in I/Q channels induce larger amplitude and phase imbalances (Fig. 5). In the 4-GHz operation band, the maximum amplitude imbalance is calculated to be 4 dB, and the maximum phase imbalance is about 40°

obtained by analyzing the I/Q signals in the calibration data group (Fig. 6). We chose 200 data in the calibration group with different frequencies and analyze the image rejection of the receiver. The minimum image rejection is only 18 dB with the I/Q imbalance induced by IF processing devices (Fig. 6). Frequency-dependent calibration parameters can be fitted with the amplitude and phase imbalances calculated from the calibration data group. We use the calibration parameters to calibrate the data in the signal data group and compensate for the residual I/Q imbalance using an impulse response filter as that used in Chi-Hao Cheng's work. After calibration, the maximum amplitude imbalance is less than 0.4 dB, and the maximum phase imbalance is less than 1.5° (Fig. 7). After I/Q imbalance calibration and compensation, the image rejection of the receiver is more than 45 dB in its 4-GHz operation bandwidth, and maximum image rejection can reach 79 dB.

Conclusions In this study, an optical delay line-based microwave photonic I/Q mixer for zero-IF receivers is proposed and experimentally demonstrated. The 90° phase shift of the LO signal is realized by tuning the optical delay line to adjust the relative transmission delay. By tuning the 90° phase shift in the microwave frequency, we build a photonic zero-IF receiver which is more stable than that in commonly used microwave photonic methods. The amplitude and phase imbalances of the I/Q channels are also minimized using wavelength-multiplexing technology. In our microwave photonic zero-IF receiver, the amplitude and phase imbalances of the I/Q channels induced by the PDs, low-pass filters, and ADCs are calibrated and compensated. After digital I/Q imbalance compensation, the zero-IF receiver based on the proposed microwave photonic I/Q mixer achieved 0.4-dB amplitude imbalance and 1.5° phase imbalance within 4-GHz operation bandwidth centered at 12-GHz frequency, and the image rejection was more than 45 dB.

Key words optical communications; microwave photon; wideband receiver; zero-intermediate frequency; image frequency rejection

OCIS codes 060.5625; 070.1170; 060.2360